

Conformational Structural Changes of Bacteriorhodopsin Adsorbed onto Single-Walled Carbon Nanotubes

Patricia Bertoncini* and Olivier Chauvet

Institut des Matériaux Jean Rouxel, Nantes Université, CNRS, 2 rue de la Houssinière, BP 32229, 44322 Nantes, France

Received: October 29, 2009; Revised Manuscript Received: January 25, 2010

The interaction between purple membranes, composed of proteins of bacteriorhodopsin (bR) and their native surrounding lipids, and single-walled carbon nanotubes (SWNT) has been investigated. In this work, sonication has been used to debundle SWNT in buffer solution without surfactant before the addition of native purple membranes. The sample was then sonicated in a bath for a short time, followed by a centrifugation. The supernatants contain proteins in excess and SWNT as individual and small bundles covered by a bR layer with an average thickness of 1.5 nm. TEM and AFM observations support the idea that only a protein monolayer surrounds the tubes. Optical absorption and infrared spectroscopy measurements provide evidence that the proteins adsorbed onto the SWNT undergo orientational changes of the helical segments in bR and helix conformational changes. We ascribe the main driving force to the hydrophobic interactions between the sidewall of the SWNT and the hydrophobic residues of the α -helices of bR.

1. Introduction

Due to their unique physicochemical properties, shape, and size, carbon nanotubes are suitable candidates for many applications, including molecular electronics, composites, and sensors. There is convincing evidence that bioelectrochemical reactions can be driven by attaching proteins to the surface of carbon nanotubes and that well-controlled aligned carbon nanotubes can be applied as immobilization matrices and as mediators for the development of biosensor devices.^{1,2} The intrinsic properties of proteins are also exploited to disperse carbon nanotubes^{3,4} or to build up controlled nanostructures onto them.⁵ In a recent study, Dorogi et al.⁶ demonstrate that a photosynthetic reaction center pigment protein complex (a redox-active enzyme in which light energy initiates a chain of intraprotein electron transport reactions) is able to attach to carbon nanotubes. It is shown that a stabilization effect of light-induced charges by CNT occurs. G. Grüner et al. report the integration of a cell membrane, containing bR, into a CNT network transistor and show that both components retain their functionality.⁷

This study shows experiments carried out with SWNT and purple membranes. These membranes consist of lipids and bacteriorhodopsin (bR) proteins at a molecular ratio of about 1:10 and are 2-dimensional crystalline arrays of bR trimers. bR is constituted by 248 residues, arranged in seven α -helices that form a cage where a retinylidene chromophore is located, as can be seen in Figure 1. bR is the key protein for the halobacterial photosynthetic capabilities, enabling the organisms to use light energy directly to drive bioenergetics' processes by the generation of a proton gradient. It is also one of the very rare molecules that occur in crystalline form in Nature. Since its discovery in 1971, bR has attracted considerable attention not only to fundamental study in the pump function but also to its potential technical applications as data storage, optical and holographic processor, photo-

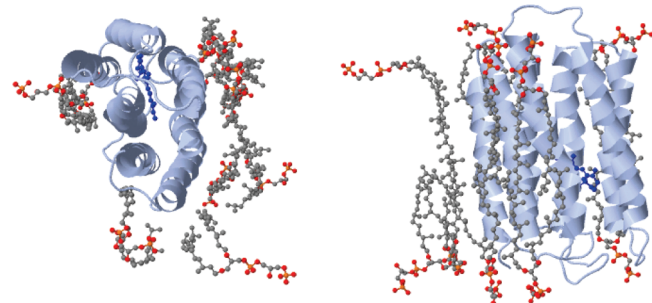


Figure 1. Top view (left) and side view (right) of schematic representations of the three-dimensional structure of bR in purple membrane (i.e., with its surrounding lipid chains). The seven α -helical bundles form a transmembrane pore. The retinylidene residue (in blue) is linked to the protein moiety via a Schiff base linkage to lysine-216.

electric and photovoltaic devices,⁸ Exploring the initial photoinduced charge transfer of photosensitive proteins like bR and aiming at the development of photochromic, photovoltaic, or charge transport devices and of biosensor applications using these proteins imply their immobilization onto solid surfaces or nanoporous materials to provide both templates and the electrodes to support the desired function. CNT can be a good material for these purposes: they are size-compatible with the proteins, have a high surface area, a good capacity to carry current and have also outstanding optical properties that can be exploited too, like the photoluminescence of individualized semiconducting SWNT.⁹ In addition, in a recent study, Jin et al. show that electronic current passes through bR-containing artificial lipid bilayers in solid "electrode-bilayer-electrode" structures as long as the retinal is present in the α -helical bundles of bR and can isomerize.¹⁰ This latest study gives indication that bR can be a stable biological system to explore electronic transport. The work described here is dedicated to the investigation of the nature and the microstructure of the interface between SWNT and bR and the protein structure itself.

* Corresponding author. E-mail: Patricia.Bertoncini@cnrs-imn.fr.

† E-mail: Olivier.Chauvet@cnrs-imn.fr.

2. Experimental Section

Commercially available HipCO SWNT have been purchased from Carbon Nanotechnologies Inc. Co. (Houston, TX) and used as received. Their diameter is 0.7–1.2 nm, as measured by transmission electron microscopy. HEPES (4-(2-hydroxyethyl)piperazine-1-ethanesulfonic acid) and NaOH (sodium hydroxide) have been purchased from Sigma-Aldrich. Suspensions of purple membranes (PM) containing wild-type bR were a courtesy gift from Dieter Oesterhelt's group at the Max-Planck Institute of Biochemistry, Martinsried, Germany.

Sample preparation was as follows: 1 mg of SWNT was first dispersed in a volume of 4 mL in a 5 mM HEPES buffer solution at pH 7.5 using an ultrasound tip for 90 min, while cooling to and maintaining the temperature at 4 °C. Then, several microliters of purple membranes (PM) were added to the SWNT dispersion, in such a way that the concentrations of bR proteins were 10, 50, or 250 nM. The dispersions were sonicated in an ice–water bath for 15 min and were finally centrifuged for 20 min at 7200 g.

The dispersions were characterized by Fourier transform Raman spectroscopy (FT-Raman) using a RFS 100 Bruker FT spectrometer and a Nd:YAG laser working at 1064 nm. For transmission electron microscopy (TEM) observations, samples were prepared by dipping a copper grid covered by a holey carbon film into 50 μL of supernatant or of PM suspension. The TEM used in this study was a Hitachi HF-2000 equipped with a field emission gun operated at 100 kV. Atomic force microscopy (AFM) images were taken with a commercial instrument (Nanoscope IIIa, Digital Instruments, Santa Barbara, CA). The scanning was performed in tapping mode with nanosensor cantilevers PPP-NCH having a nominal force constant of about 42 N/m and resonance frequency of about 330 kHz. For the sample preparation, 10 μL of supernatant or of PM suspension were deposited onto a freshly cleaved mica surface for 10 min. Afterward, the surface was rinsed with nanopure water and dried under a stream of nitrogen. In the case of image E in Figure 4, the same procedure was followed using 20 μL of the suspension and a time deposition of 15 min. UV-vis–NIR absorption spectra of the dispersions were recorded on a CARY 5G UV-vis–NIR spectrometer. To perform attenuated total reflection Fourier transform infrared spectroscopy (ATR-FTIR), 1 μL of a suspension was deposited on the internal reflection element (IRE) surface and the solvent was slowly evaporated under a nitrogen flow while a pipet tip was used to spread the liquid over the useful surface of the IRE to make the film as uniform as possible. Spectra were measured at room temperature on a FTIR Bruker Vertex 70 spectrometer equipped with an ATR stage. Spectra were recorded at a resolution of 2 cm⁻¹.

3. Results and Discussion

Figure 2 displays the Raman/emission spectra of raw SWNT and a supernatant in which the concentration of native bR membranes initially introduced in the SWNT dispersion was 10 nM. These spectra have been obtained with an excitation line at 1064 nm. This excitation line corresponds to allowed optical E11 transitions of semiconducting SWNT. The Raman resonant peaks are labeled with stars in Figure 2. The two main peaks are due to the radial breathing mode (at 268 cm⁻¹) and to the tangential G modes close to 1590 cm⁻¹. The peak close to 2551 cm⁻¹ is the second-order D' mode. There is no significant modification of the Raman line positions within our experimental accuracy. More interestingly, it can be noticed that two broad lines found around 550 and 1500 cm⁻¹ (below the

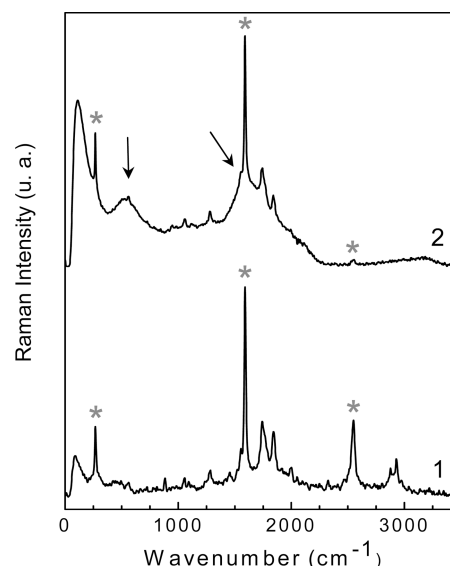


Figure 2. Raman/emission spectra of SWNT/bR hybrids (2) and raw SWNTs dispersed in ethanol (1). The spectra have been obtained with an excitation line at 1064 nm. The stars refer to the Raman resonant peaks of the SWNT. The arrows indicate NIR fluorescence lines.

Raman G lines) are appearing (indicated by arrows in Figure 2). These lines correspond to fluorescence lines associated to the NIR emission of semiconducting SWNT, according to the pioneering work of O'Connell et al.¹¹ The NIR emission is observed for isolated semiconducting SWNT only. In fact, when the nanotubes are embedded in bundles, the emission is quenched as soon as the bundle contains metallic nanotubes. The fluorescence comes from the radiative decay of the excitons formed after the absorption of the E11 photon. Each kind of SWNT should thus give a specific fluorescence line. Here, the lines at 554 and 1556 cm⁻¹ may be attributed to (9,2) and (11,1) SWNT according to Bachilo et al.¹² It is noteworthy that as produced nanotubes are embedded in nonfluorescent bundles. In aqueous media, even if ultrasonication is able to destroy the bundle organization, the hydrophobicity of the carbon surface results usually in the bundle reformation. It is quite difficult to stabilize individual (and thus fluorescent) nanotubes in the aqueous environment. Our observation shows that individualized carbon nanotubes are present in the supernatants. It is only possible when nanotubes are interacting with the protein.

Several TEM micrographs are shown in Figure 3. In Figure 3A–C, thin films of proteins are spanning over the carbon film of the grid. SWNT are embedded within these films as individual tubes or bundles. In addition, superimposed platted sheets with lateral dimensions up to several hundreds of nanometers are observed, as can be seen in Figure 3C (indicated by arrows) and Figure 3D,E. These sheets have, in many cases, a particular shape with well-defined angles and are crystallized in a hexagonal lattice, as revealed by electron diffraction (patterns not shown). We attribute these sheets to bR protein lattices, according to the fact that native purple membrane (PM) forms two-dimensional lattices¹³ as well as delipidated PM.^{14,15} Electron beam damage was evident after prolonged observation of a single area of the protein film, causing the formation of rapidly enlarging holes in the protein films.

Another preparation of the TEM grids, in which we used the samples before centrifugation as starting material, permits us to visualize individual SWNT. Figure 4 shows typical micrographs of individual single-walled carbon nanotubes onto which bR have been successfully immobilized noncovalently. The

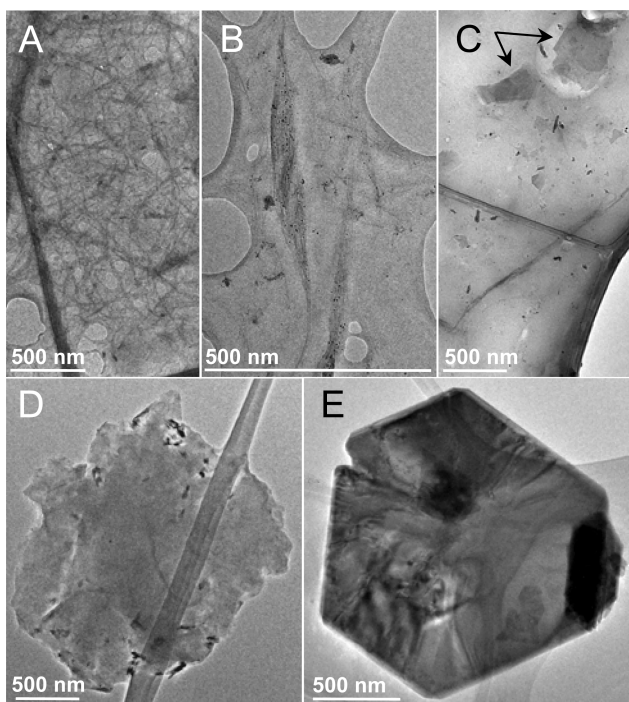


Figure 3. (A)–(C) Transmission electron micrographs at 100 kV of protein films embedding SWNT. The arrows indicate bR sheets. (D) and (E) Platted sheets of bR.

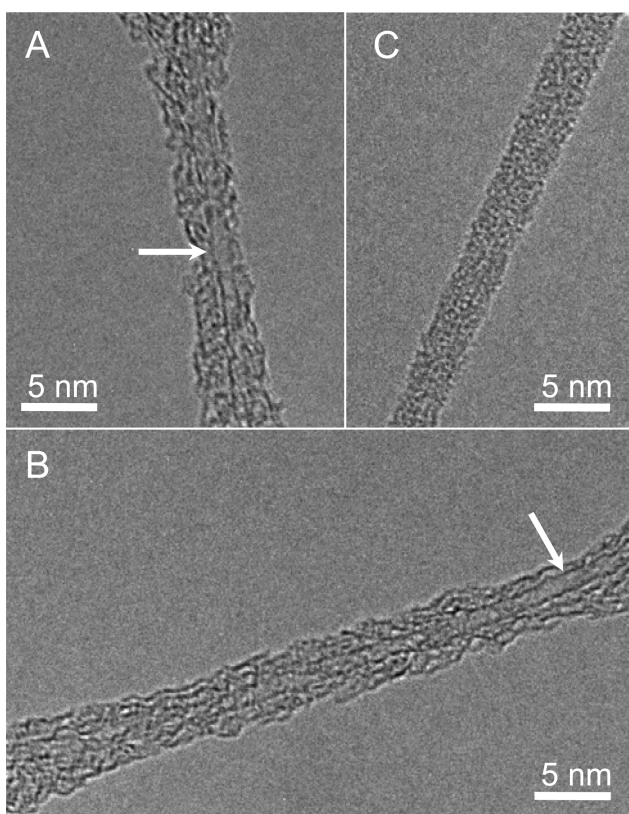


Figure 4. Transmission electron micrographs taken at 100 kV showing individual single-walled carbon nanotubes coated with bR molecules. White arrows show the sidewall of the nanotubes.

carbon nanotubes in Figure 4A,B have a diameter around 0.9 and 1.1 nm and are covered by a protein layer of 1–1.5 nm. The whole diameter of the hybrids is around 4–5 nm. The elongated object that can be seen in Figure 4C is therefore attributed to a single-walled carbon nanotube covered by

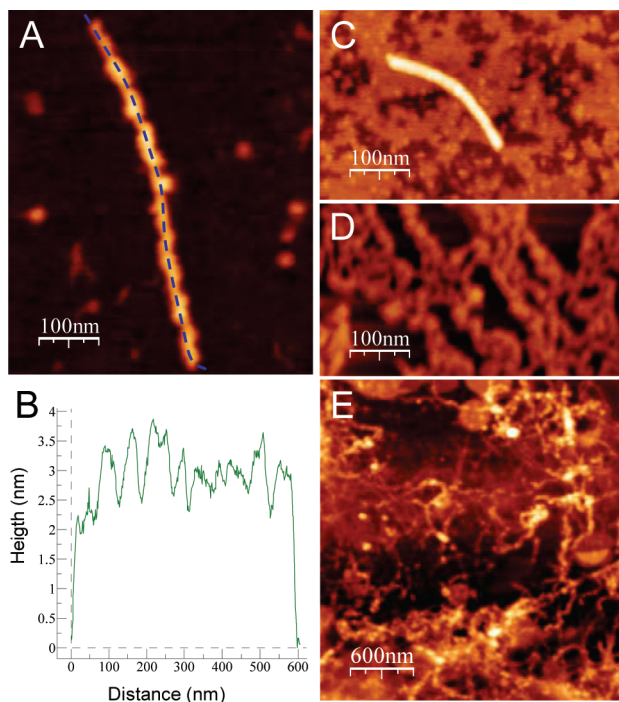


Figure 5. (A) and (C) AFM topographs showing individual SWNT/bR complexes and bR proteins deposited onto a mica surface, respectively. Full color Z-scale: 5 nm. (B) Section analysis profile along the dashed blue lines on image A. (D) AFM topograph showing bR proteins deposited onto a HOPG surface. Full color Z-scale: 5 nm. (E) AFM topograph showing SWNT/bR hybrids and bR proteins deposited onto a mica surface. Full color Z-scale: 40 nm.

proteins too. These observations are consistent with the formation of SWNT/bR hybrids and confirm the presence of individualized carbon nanotubes, in agreement with the Raman spectroscopy measurements.

Atomic force microscopy (AFM) images of rinsed films supernatants are shown in Figure 5. Isolated SWNT/bR hybrids can be seen on top of flat mica surfaces that are partially covered by bR proteins in Figure 5A,C. The height profile obtained along the dashed blue line drawn in Figure 5A is shown in Figure 5B. It is irregular due to the presence of the proteins. Since the upper carbon nanotube surface appears at a height value of approximately 2 nm, there are some proteins under the nanotube, and the protein layer has a thickness of 1.5–2 nm, consistent with the TEM observations. To get more insight about the structure of the hybrids, diluted native bR membranes were deposited onto freshly cleaved highly oriented pyrolytic graphite (HOPG) surfaces and imaged in air. One typical AFM image is shown in Figure 5D. As can be seen, the proteins do not cover completely the surface of the substrate. The average height of this bR layer is 1.5 nm (± 0.3 nm). This can be compared to the 5 nm height of a PM-bR sheet and to the protein layer thickness of 1.5 nm found on the nanotube surface. This suggests that the α -helices of the bR proteins interact with the sidewall of the nanotubes or the graphite surface, providing evidence that the main driving force of the coupling can be attributed to hydrophobic interactions. Note that the lengths of the carbon nanotubes are relatively short, less than 800 nm in general (in Figure 5A,C, the lengths are 247 and 590 nm, respectively). This is likely due to the sonication step used to disperse the carbon nanotubes in the buffer solution before the introduction of the PM-bR and the centrifugation step. An AFM image of a rinsed film of supernatant deposited on mica is shown in Figure 5E. In this case, larger amounts of supernatant were deposited

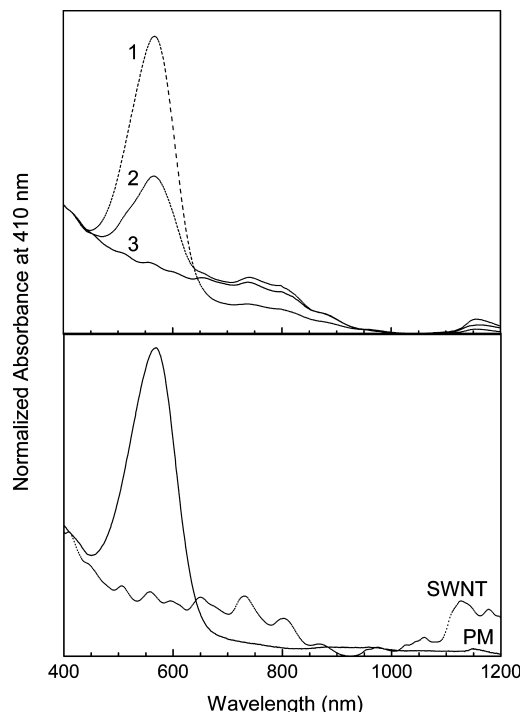


Figure 6. Upper panel: UV-visible absorption spectra of supernatants containing SWNT/BR hybrids between 400 and 1200 nm. The initial protein concentrations added to the SWNT dispersions are 10 nM (spectrum 3, solid line), 50 nM (spectrum 2, short dashed line), and 250 nM (spectrum 1, dashed line). Bottom panel: UV-visible spectra of native bR (solid line) and well-dispersed SWNT by anionic surfactant molecules of sodium dodecylbenzenesulfonate (short dotted line). The optical absorbance is normalized at a wavelength of 410 nm for all spectra.

onto the mica surface and for a longer time, as described in the Experimental Section. Many SWNT/bR hybrids intermingle, and small aggregates of proteins and bR patches with lateral dimensions up to several hundreds of nanometers can be seen. These results are in good agreement with those obtained by TEM.

UV-visible spectra of different supernatants containing the SWNT/bR hybrids and bR are presented in the upper part of the Figure 6. Spectra 1–3 correspond to three samples in which the concentrations of bR membranes in the SWNT dispersions before the centrifugation step were respectively 250, 50, and 10 nM. For comparison, a spectrum of a dispersion of SWNT by a surfactant (sodium dodecylbenzenesulfonate) in which separated absorption features characteristic of well-dispersed SWNT can be seen¹¹ and a spectrum of native bR membranes are also shown in the bottom of Figure 6. Native bR absorbs at a maximum of 568 nm in the region between 400 and 1200 nm. In Figure 6, the absorption peak corresponding to bR proteins and the features corresponding to SWNT are clearly identifiable on the absorption spectra of supernatants containing large amounts of bR proteins (spectra 1 and 2). For supernatants containing the lower amount of proteins, the absorption signature of the SWNT is the only one visible in spectrum 3. The absorption features of the SWNT are broader and less defined compared with those observed on well-dispersed SWNT by the surfactant, indicating that SWNT in the supernatants are less individualized and can be present as small bundles, in agreement with the TEM observations. The absorption peaks of bR in case of spectra 1 and 2 are blue-shifted by ~2 and ~5 nm, indicating that there are small changes in the retinal environment for a large amount of bR proteins in the supernatants. These blue

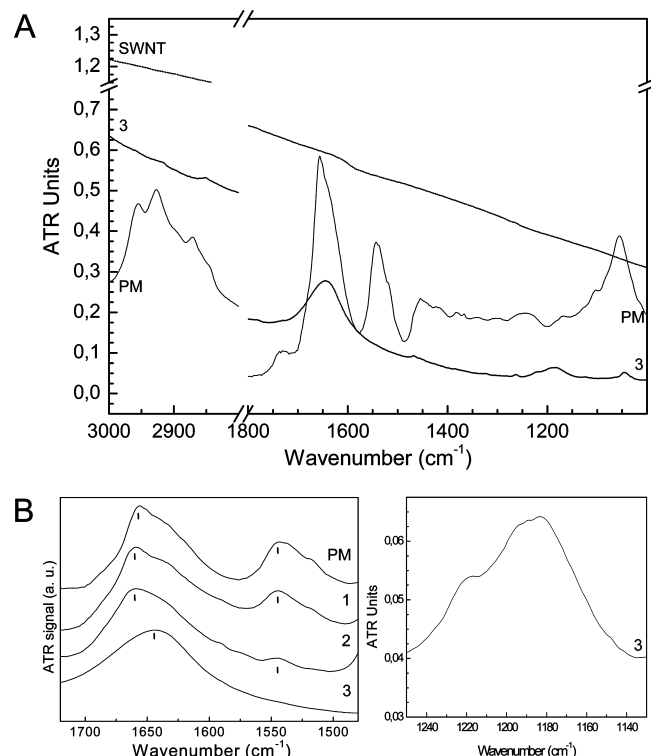


Figure 7. (A) Infrared spectra in the 3000–2800 and 1800–1000 cm⁻¹ regions of a native purple membrane film dried from a 0.6 mg·mL⁻¹ aqueous suspension (solid line), of a SWNT HipCO powder (dotted line), and of a film cast from a supernatant containing SWNT/bR hybrids and bR proteins (dashed line, spectrum 3). (B) Left panel: amide I and amide II regions (1720–1480 cm⁻¹) of films of native bR membranes and of three supernatants containing different amounts of bR. Spectra were normalized in the range 1720–1480 cm⁻¹ before being translated vertically for a better visualization. Initial protein concentrations added to the SWNT dispersions were 10 nM (spectrum 3), 50 nM (spectrum 2), and 250 nM (spectrum 1). Right panel: details of spectrum 3 in the region between 1250 and 1130 cm⁻¹ corresponding to the C=C stretching modes of the chromophore.

shifts of the retinal absorption are in favor of a partial loss of the native lipids surrounding the bR proteins.^{16–19} Indeed, the UV-visible spectra prove that the protein and the SWNT have maintained most of their optical properties in the dispersion.

bR protein conformational changes after being adsorbed onto single-walled carbon nanotubes were investigated at room temperature by attenuated total reflection FOURIER transform infrared spectroscopy (ATR-FTIR). Figure 7A displays infrared spectra of films cast either from a native bR membrane suspension or from a supernatant containing SWNT/bR hybrids and bR-proteins (in which the concentration of native bR membranes introduced in the SWNT dispersions before the centrifugation step was 10 nM) and a SWNT HipCO powder. The ATR-FTIR spectrum of PM suspension is in good agreement with previous reports.^{20–22} The region from 3000 to 2800 cm⁻¹, corresponding to C–H stretching modes exhibits three intense bands centered at 2955, 2927, and 2870 cm⁻¹ that arise primarily from the native lipid chains. The region between 1700 and 1500 cm⁻¹ shows essentially two intense features with maxima positioned at 1656 and 1643 cm⁻¹, corresponding to the amide I and amide II stretching modes, respectively, and related to the secondary structure of bR composed essentially of α_I - and α_{II} -helices.^{23,24} The spectral region between 1500 and 1000 cm⁻¹ is composed of modes arising from amino acid residues in bR and from vibrational modes of the purple membrane lipids. The regions assigned in the C=C stretching

modes ($1600\text{--}1500\text{ cm}^{-1}$) and in the C–C stretching modes ($1250\text{--}1150\text{ cm}^{-1}$) correspond to the retinylidene chromophore. The ATR FT-IR spectrum of raw SWNT gives rise to a featureless monotonically increasing absorption in the spectral region between 3000 and 400 cm^{-1} , which is associated with the π -plasmon of the SWNT. This featureless baseline of SWNT is superimposed on the absorption features of native bR membranes, as can be clearly seen on curve 3 in Figure 7A. Therefore, structural changes in the backbone of bR molecules can be discerned. Moreover, complementary information can be obtained about the presence of the lipids as well as about the chromophore environment.

Spectra of three different supernatants containing SWNT/bR hybrids and bR proteins (spectra 1–3 for concentrations of native bR membranes in the SWNT dispersions before the centrifugation step of respectively 250, 50, and 10 nM) are displayed in Figure 7B (left) in the amide I and amide II regions. Shapes and positions at maximum of the stretching frequencies depend on the amount of bR in the supernatants. For the sample containing the larger amount of bR proteins, the amide I and amide II stretching frequencies are less modified than for native bR membranes: a slight increase of intensity on the higher energy side of the amide I band can be seen, and the maximum of the peak is centered at 1660 cm^{-1} . There is no change in position for the amide II N–H band centered at 1543 cm^{-1} . Shape and position are close to those measured on partially delipidated proteins.^{16,20} This is supported by the analysis of the C–H stretching region composed primarily of modes arising from the lipids (data not shown). In fact, the ratio of the integrated intensity of the C–H vibrational region (composed primarily of lipid stretching modes) to the integrated intensity of the amide I region has a value of 0.75 instead of 0.84 for native bR membranes, indicating a loss of lipids. This is in agreement with the results obtained by UV-visible spectroscopy as described previously. Amide I and amide II regions of the films cast from supernatants and containing lower amounts of proteins exhibit large changes. For the sample containing the lower amount of bR proteins (spectrum 3 in Figure 7B (left)), the amide I stretching frequency peak is centered at $\sim 1644\text{ cm}^{-1}$, i.e., shifted by $\sim 12\text{ cm}^{-1}$ compared with that for native bR membranes and the amide II band is completely missing. Relative dichroic ratios of the amide I and amide II modes may give information about the type of the α -helix in membrane proteins. They are also highly dependent on the α -helix length.²⁵ Previous studies report a decrease in intensity of the amide II mode relative to the amide I mode and a downshift of the amide I frequency of several cm^{-1} when there is a conversion from the α_{II} - to the α_I -helical structures: 6 cm^{-1} is observed for bR membranes exposed to Triton X-100²⁰ and for bR-monomers solubilized by *n*-octyl- β -glucoside²⁶ or by 3-[*(3*-cholamidopropyl)dimethylammonio]-1-propanesulfonate (CHAPS)¹⁶ and 10 cm^{-1} for bR monomers solubilized using Triton X-100.¹⁶ Our observation of a 12 cm^{-1} shift is thus compatible with a modification of the α -helical structure.

Spectrum 2 in Figure 7B (left) corresponds to a sample in which the concentration of native membranes initially introduced was 50 nM, an intermediate value compared with those previously discussed. The maximum of the amide I peak is at 1660 cm^{-1} , but the shape is different and a decrease in the intensity of the amide II mode relative to the amide II mode is clearly visible. These results can be interpreted by the coexistence in the supernatants of two main bR protein conformations. The first one corresponds to partially delipidated bR proteins with an amide I stretching frequency at 1660 cm^{-1} , supported

also by the presence of hexagonal crystalline structures observed by TEM. The other one may correspond to bR in which α_{II} -helices convert to α_I -helices and/or in which changes in helix conformation happen with an amide I stretching frequency of 1644 cm^{-1} . The proportion of both conformations differs significantly as a function of the amount of native bR membranes initially introduced: the more bR proteins are introduced, the higher the conformation corresponding to delipidated proteins. The conformation in which the protein secondary structure is the most affected compared with native bR membranes is attributed to the proteins that adsorbed onto the sidewall of the SWNT.

Figure 7B (right) shows the spectrum of sample 3 in the region $1250\text{--}1130\text{ cm}^{-1}$. This region corresponds to C–C stretching modes of the retinylidene chromophore. Comparatively to the ATR spectrum of dried native bR membranes, a pronounced absorption band with a maximum centered at 1182 cm^{-1} can be seen, indicating important changes in the retinal environment.

Several studies about the functionalization of SWNT by peptides provide strong evidence that hydrophobic and in particular aromatic residues may interact strongly with SWNT.^{27–30} Since a large number of residues in the bR α -helices are hydrophobic and aromatic residues are present in large amounts, the main driving force of the immobilization of bR onto SWNT may be assigned to hydrophobic and van der Waals interactions between the sidewall of the nanotube and some hydrophobic residues of bR α -helices. When adsorbed onto the sidewall of the SWNT, bR undergoes important conformational structural changes, as demonstrated by the downshift of the amide I mode of $\sim 12\text{ cm}^{-1}$ and the missing peak of the amide II mode. These findings are consistent with orientational and/or conformational changes of the helical segments in bR. Both effects may probably happen. This idea is supported by a recent theoretical work, in which Chiu et al. shows that a peptide helix may curve to match the cylindrical water/SWNT interface, allowing the peptide to maintain its α -helical structure on the SWNT surface.³¹

We expect that the structural changes in bR will influence the function of bR and its photocycle. For example, a study of Wang et al. shows that the protein aggregation state (native trimeric state) is important in controlling the photocycle kinetics¹⁷ and Rödig et al. report molecular changes during intermediates of bR.³²

4. Conclusion

This study provides evidence that the membrane bR proteins can be immobilized onto SWNT through hydrophobic interactions between the bR α -helices and the sidewall of the nanotube. The TEM and AFM study presented here supports the idea that only one protein layer surrounds the tubes. When adsorbed onto SWNT, bR proteins undergo important secondary structural changes, as demonstrated by the red shift of 12 cm^{-1} of the amide I band and the modification of the amide II related profile in the ATR-FTIR measurements. These results may be explained by orientational changes of the helical segments in bR as well as changes of the helix conformation through the functionalization of the SWNT and through a loss of protein–protein interactions and lipid–protein interactions. It is noteworthy that this noncovalent functionalization allows us to stabilize individual nanotubes in an aqueous medium. The absorption of bR onto the sidewall of the SWNT that exhibit their intrinsic electronic and optical properties and the presence of the retinal inside the bR α -helical bundles attested by the vibrational

spectroscopy measurements were the first prerequisites to built new devices. We are focusing our interest on the photophysical properties of bR in contact with SWNT and on the synthesis of new hybrids made of SWNT and bR to investigate their photoresponse and evaluate their potential use as building blocks for molecular optoelectronic devices.

Acknowledgment. Suspensions of PM containing wild-type bR were a gift from Dieter Oesterhelt's group at Max-Planck Institute of Biochemistry, Martinsried, Germany.

References and Notes

- (1) Gong, K.; Yan, Y.; Zhang, M.; Su, L.; Xiong, S.; Mao, L. *Anal. Sci.* **2005**, *21*, 1383.
- (2) Willner, B.; Katz, E.; Willner, I. *Curr. Opin. Biotechnol.* **1996**, *17*, 589.
- (3) Matsuura, K.; Saito, T.; Okazaki, T.; Ohshima, S.; Yumura, M.; Iijima, S. *Chem. Phys. Lett.* **2006**, *429*, 497.
- (4) Nepal, D.; Geckeler, K. E. *Small* **2007**, *3*, 1279.
- (5) Kurppa, K.; Jiang, H.; Szilvay, G. R.; Nasibulin, A. G.; Kauppinen, E. I.; Linder, M. B. *Angew. Chem., Int. Ed.* **2007**, *46*, 6446.
- (6) Dorogi, M.; Balint, Z.; Miko, C.; Vileno, B.; Milas, M.; Hernadi, K.; Forro, L.; Varo, G.; Nagy, L. *J. Phys. Chem. B* **2006**, *110*, 21473.
- (7) Bradley, K.; Davis, A.; Gabriel, J.-C. P.; Grüner, G. *Nano Lett.* **2005**, *5*, 841.
- (8) Hamp, N. *Chem. Rev.* **2000**, *100*, 1755.
- (9) Lefebvre, J.; Maruyama, S.; Finnie, P. *Top. Appl. Phys.* **2008**, *111*, 287.
- (10) Jin, Y.; Friedman, N.; Sheves, M.; He, T.; Cahen, D. *Proc. Natl. Acad. Sci. U.S.A.* **2006**, *103*, 8601.
- (11) O'Connel, M. J.; Bachilo, S. M.; Huffman, C. B.; Moore, V. C.; Strano, M. S.; Haroz, E. H.; Rialon, K. L.; Boul, P. J.; Noon, W. H.; Kittrell, C.; Ma, J.; Hauge, R. H.; Weisman, R. B.; Smalley, R. E. *Science* **2002**, *297*, 593.
- (12) Bachilo, S. M.; Strano, M. S.; Kittrell, C.; Hauge, R. H.; Smalley, R. E.; Bruce, W. R. *Science* **2002**, *298*, 2361.
- (13) Henderson, R. *J. Mol. Biol.* **1975**, *93*, 123.
- (14) Fukuda, K.; Ikegami, A.; Nasuda-Kouyama, A.; Kouyama, T. *Biochemistry* **1990**, *29*, 1997.
- (15) Glaeser, R. M.; Jubb, J. S.; Henderson, R. *Biophys. J.* **1985**, *48*, 775.
- (16) Heyes, C. D.; El-Sayed, M. A. *J. Biol. Chem.* **2002**, *277*, 29437.
- (17) Wang, J.; Link, S.; Heyes, C. D.; El-Sayed, M. A. *Biophys. J.* **2002**, *83*, 1557.
- (18) Tan, E. H. L.; Birge, R. R. *Biophys. J.* **1996**, *70*, 2385.
- (19) Tanio, M.; Tuzi, S.; Yamaguchi, S.; Konishi, H.; Naito, A.; Needleman, R.; Lanyi, J. K.; Saito, H. *Biochim. Biophys. Acta* **1998**, *1375*, 84.
- (20) Barnett, S. M.; Dracheva, S.; Hendler, R. W.; Levin, I. W. *Biochemistry* **1996**, *35*, 4558.
- (21) Rothschild, K. J.; Clark, N. A. *Biophys. J.* **1979**, *25*, 473.
- (22) Marrero, H.; Rothschild, K. J. *Biophys. J.* **1987**, *52*, 629.
- (23) Krimm, S.; Dwivedi, A. M. *Science* **1982**, *216*, 408.
- (24) Dwivedi, A. M.; Krimm, S. *Biopolymers* **1984**, *23*, 923.
- (25) Reisdorf, W. C., Jr.; Krimm, S. *Biophys. J.* **1995**, *69*, 271.
- (26) Sonoyama, M.; Hasegawa, T.; Nakano, T.; Mitaku, S. *Vibr. Spectrosc.* **2004**, *35*, 115.
- (27) Wang, S. Q.; Humphreys, E. S.; Chung, E. S.; Delduco, D. F.; Lustig, S. R.; Wang, H.; Parker, K. N.; Rizzo, N. W.; Subramoney, S.; Chiang, Y.-M.; Jagota, A. *Nat. Mater.* **2003**, *2*, 196.
- (28) Zorbas, V.; Smith, A. L.; Xie, H.; Ortiz-Acevedo, Dalton, A. B.; Dieckmann, G. R.; Draper, R. K.; Baughman, R. H.; Musselman, I. H. *J. Am. Chem. Soc.* **2005**, *127*, 12323.
- (29) Sharma, R.; Mc Namara, J. P.; Raju, R. K.; Vincent, M. A.; Hillier, I. H.; Morgado, C. A. *Phys. Chem. Chem. Phys.* **2008**, *10*, 2767.
- (30) Wang, Y.; Ai, H. *J. Phys. Chem. B* **2009**, *113*, 9620.
- (31) Chiu, C.-C.; Dieckmann, G. R.; Nielsen, S. O. *J. Phys. Chem. B* **2008**, *112*, 16326.
- (32) Rödig, C.; Chizhov, I.; Weidlich, O.; Siebert, F. *Biophys. J.* **1999**, *76*, 2687.

JP9103432